

INFLUENCE OF GEOMETRY AND LOAD CASE ON THE LOCAL STRESS STATE IN WIDE PLATES WITH SEMI ELLIPTICAL SURFACE CRACKS

F. Grimpe and W. Dahl\*

Three dimensional elastic plastic finite element analyses of wide plates with surface cracks have been performed to investigate the dependence of the local stress state and the crack initiation locus on the geometry and on the load case. The local constraint, the strain and the distribution of J-integral have been analysed along the crack front of single surface cracked tension (SSCT) and single surface cracked bending (SSCB) plates.

INTRODUCTION

When the local stress field and the distribution of the J-integral along the crack front of a structural component is known for the state of crack initiation one can predict the initiation locus. For that purpose three dimensional elastic plastic finite element (FE) analyses of wide plates with regard to the local loading situation have been performed. The most frequent type of crack in structure components is a surface crack. Therefore the analysed plates had surface cracks of a wide range of flaw geometries.

FINITE ELEMENT ANALYSES

For the systematic investigation it was necessary to analyse plates with different crack depth (a) and crack form (a/c) according to figure 1. For these calculations a

\* Institute of Ferrous Metallurgy, Technical University Aachen, Germany

meshing algorithm was developed and build in a program which generates finite element models for very different geometries (1). The displacement controlled calculations were carried out by using the FE-program Abaqus (2). Because of the symmetry it is sufficient to model a quarter of the plates only. All models consist of 3380 nodes forming 688 isoparametric elements with 20 nodes and reduced integration. Minimum element size is 0.1mm. There are six elements around and eight elements along the crack front. The elements around the crack tip are collapsed to produce an  $1/r$  singularity (3). A typical mesh is to be seen in figure 1. The J-integral was determined according to (4).

The material properties are those of a high strength structural steel Fe 690. They were given as a multilinear true stress strain curve for quasistatic loading with  $\sigma_y=736\text{MPa}$ , Young's modulus (210000MPa) and Poisson's ratio (0.3).

All plates had a length  $L=720\text{mm}$ , a width  $W=300\text{mm}$  and a thickness  $t=30\text{mm}$ . Two different crack depths were analysed:  $c=15\text{mm}$  ( $a/t=0.50$ ) and  $c=3.4\text{mm}$  ( $a/t=0.11$ ). Three different crack forms were calculated:  $a/c=0.2, 0.6, 1.0$ . The load cases were tension (SSCT) and four point bending (SSCB4).

## RESULTS

The local quantities described below are the stress triaxiality  $h$  (ratio of hydrostatic stress to equivalent stress) as a constraint parameter, the equivalent plastic strain  $\epsilon_{eq}$  and the J-integral. In the following figures the values are plotted along the crack front in the distance where the stress triaxiality had its maximum. The x-axis shows the angle  $\phi$  which is explained in figure 1. The analyses are all made for the state of crack initiation which was assumed to take place when the average J-integral along the crack front reached the experimental  $J_i$  value of the material which is  $J=95\text{ N/mm}$ .

The distribution of  $h$  along the crack front is plotted in figure 2. The highest values are calculated for  $a/c=0.2$ . The courses are similar. But for the shallow cracks ( $a=3.4\text{mm}$ )  $h$  decreases with increasing angle right from the beginning. The deep cracks ( $a=15\text{mm}$ ) have a constant value of  $h$  up to  $75^\circ$ . For all geometries the highest constraint is at the deepest point of the crack.

As to be seen in figure 3 the crack depth influences the strain in particular between  $50$  and  $90^\circ$ . For  $a=3.4\text{mm}$  the strains are nearly constant along the crack front. The deep cracks show different tendencies in this area depending on the crack form.

For  $a/c=1.0$  the strain decreases up to a point close to the plates surface. The crack forms  $a/c=0.6$  and  $a/c=0.2$  show increasing strain courses.

The distribution of  $J$  along the crack front is plotted in figure 4. While all  $J$ -curves of the shallow cracks are decreasing with increasing angle the  $J$ -courses for the deep cracks show different tendencies. For the long crack form ( $a/c=0.2$ )  $J$  decreases. The maximum is at the deepest point of the crack. The crack with  $a/c=0.6$  has a nearly constant value up to  $75^\circ$ . Then it decreases. The maximum is again at  $0^\circ$ . The half circular flaw ( $a/c=1.0$ ) has a maximum at  $70^\circ$ . This is the only flaw that yields a  $J$  maximum outside the middle of the crack front. An explanation for the distribution of  $J$  is possible by taking into account both: the local stresses and strains. For the shallow crack the triaxiality decreases along  $\phi$  while the strains are constant. This leads to decreasing  $J$  courses. In the case of the deep crack  $h$  is constant up to  $70^\circ$  and then decreases. The strain for  $a/c=0.2$  decreases, too. That yields a falling  $J$ -course. For  $a/c=0.6$  strain and  $J$ -integral are nearly constant. Only for  $a/c=1.0$  strain rises and that leads together with a constant or slightly falling triaxiality to the above mentioned  $J$  maximum at  $70^\circ$  for the deep half circular flaw.

The influence of the load case is shown in figure 5. The distribution of  $J$  for a crack of  $a=15\text{mm}$  under four point bending (SSCB4) is to be seen. The course for  $a/c=0.2$  is constant for bending while it was decreasing for tension (figure 4). The other crack forms have a markable maximum at  $80^\circ$  in the case of bending.

Again the contribution of stresses and strains explains the  $J$  curves. The courses of the triaxiality are decreasing for all crack forms (figure 6) while the slope of the increasing strains becomes steeper with increasing ratio  $a/c$  (figure 7).

#### CONCLUSIONS

There is a strong influence of geometry and load case on the local state of stress and strain. The contribution of stress and strain determines the local distribution of  $J$ . In all investigated cases the triaxiality  $h$  has its maximum at the deepest point of the crack. The experimentally observable „canoeing effect“ in crack growth can not be explained by the courses of the triaxiality. In opposit to the results of (5) and (6) no „canoe effect“ in terms of  $h$  was found. A reason seems to be that in these investigations special geometries with surface cracks were analysed like curved plates and side grooved specimens. In usual surface cracked wide plates as they were investigated in this work only for the  $J$ -integral there are cases with a maximum outside the deepest point. These are geometries with large  $a/c$  ratios in particular under bending load.

REFERENCES

- (1) Grimpe, F.; Dahl, W., „Using Abaqus to Investigate Local Stress Fields and Toughness Requirements in Surface Cracked Tension Plates“, Abaqus User´s Conference, 31. May-02. June 1995, Paris, France, proc. , p. 321/334
- (2) Hibbitt, H. D. et al., „Abaqus User´s Manual Version 5.4“ (1994), Pawtucket, Rhode Island, USA
- (3) European Structural Integrity Society (ESIS), „Recommendations for Use of FEM in Fracture Mechanics“, ESIS Newsletter Nr. 15 (1991), p. 3/5
- (4) Parks, D. M., „The Virtual Crack Extension Method for Nonlinear Material Behaviour“, Comp. Meth. Appl. Mech. Eng. 12 (1977), p. 353/364
- (5) Aurich, D.; Sommer, E., „The Effect of Constraint on Elastic-plastic Fracture“, Steel Research 59 (1988), No. 8, p. 358/367
- (6) Moussavi Zadeh, G. et al., „The Importance of the Triaxiality Modified J Concept for the Assessment of Pressurized Components With Surface Flaws“, Nuclear Engng. & Design 157 (1995), p. 111/121

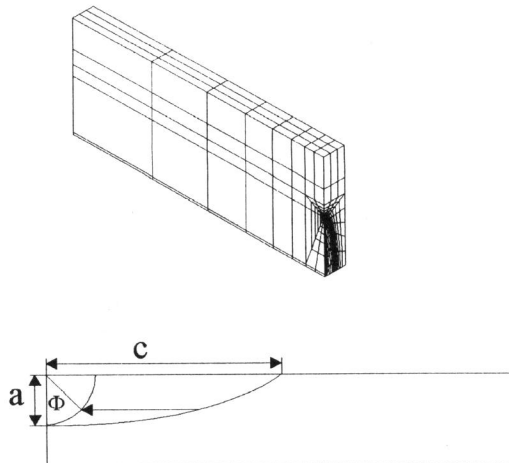


Figure 1. Finite element mesh and crack parameters

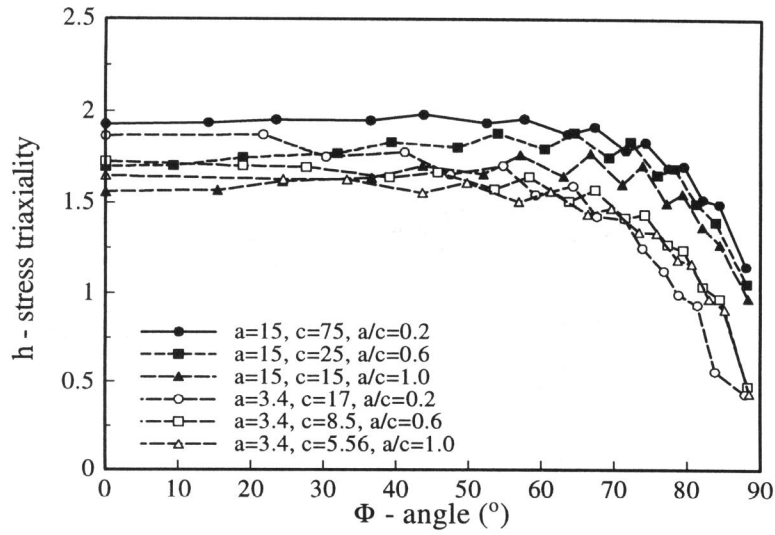


Figure 2. Triaxiality along crack front (SSCT)

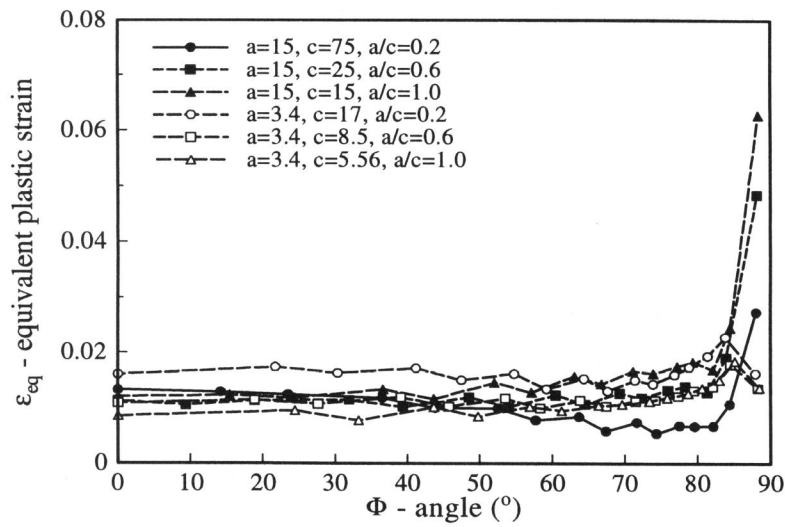


Figure 3. Equivalent plastic strain along crack front (SSCT)

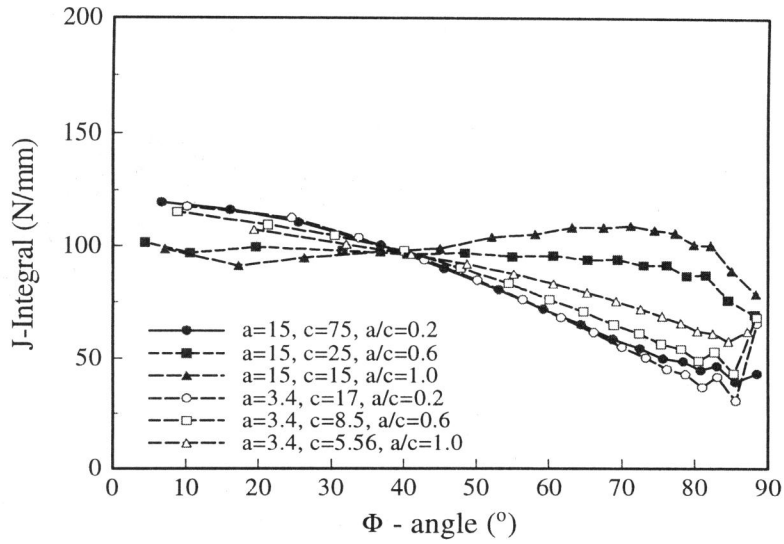


Figure 4. J-integral along crack front (SSCT)

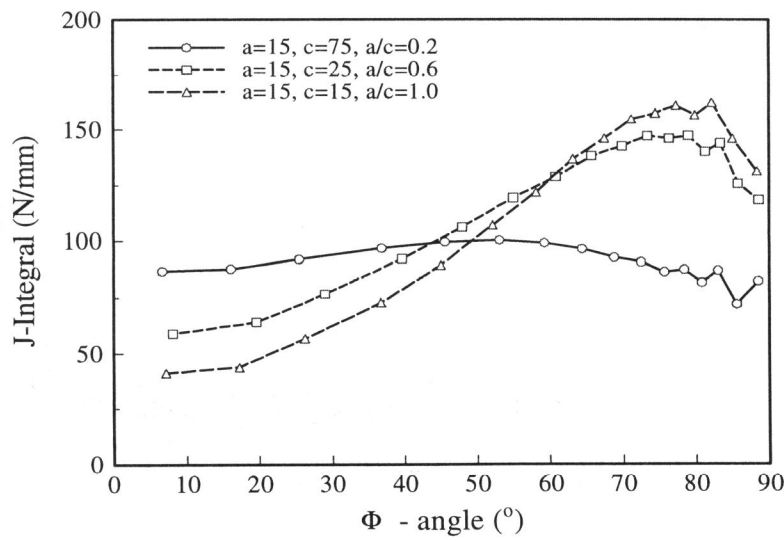


Figure 5. J-integral along crack front (SSCB4)

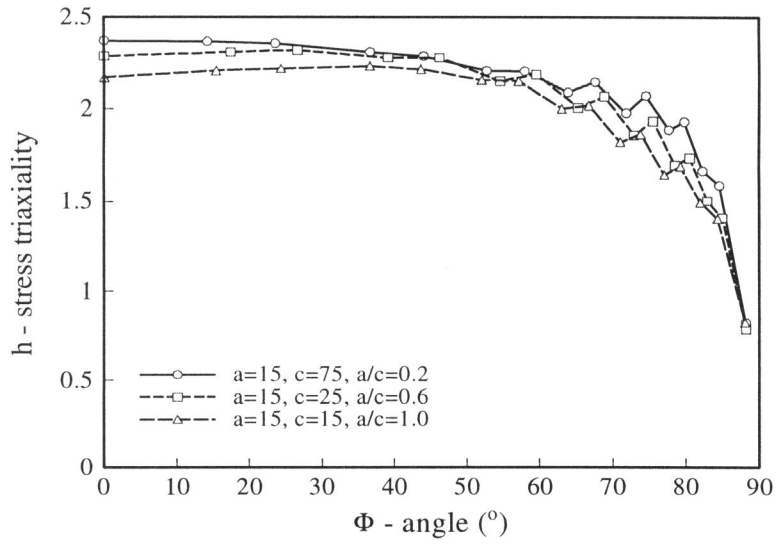


Figure 6. Triaxiality along crack front (SSCB4)

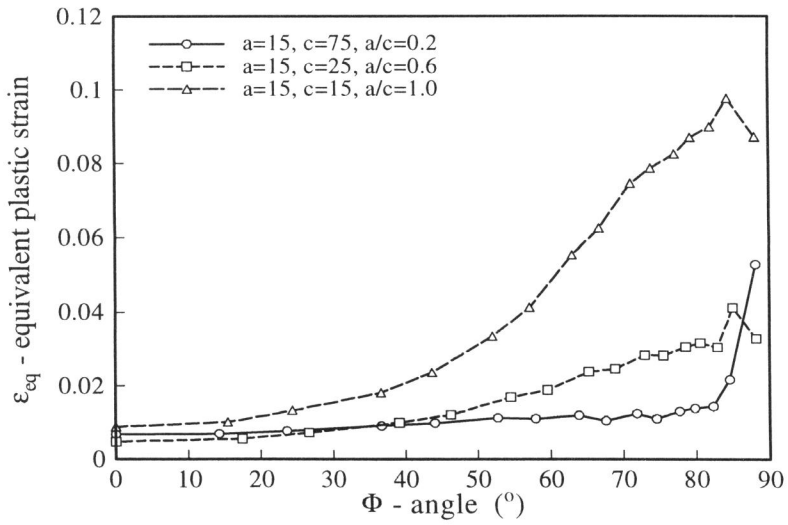


Figure 7. Equivalent plastic strain along crack front (SSCB4)